Low energy optical model studies of proton scattering on ^{54}Fe and ^{56}Fe

N. Boukharouba,* C. E. Brient, S. M. Grimes, V. Mishra,† and R. S. Pedroni‡
Ohio University, Athens, Ohio 45701
(Received 27 March 1992)

Proton elastic and inelastic cross sections have been measured at a number of energies between 3.73 and 7.74 MeV on targets of ^{54}Fe and ^{56}Fe. The (p,γ) cross section was measured at the same energies. Coupled-channel effects on the absorption cross sections are examined and an analysis in terms of dispersion theory is presented. A good representation of single particle energies was obtained. Calculations of two-particle–one-hole state densities agree qualitatively with the imaginary potential differences, in that shell effects disappear above the Coulomb barrier.

PACS number(s): 25.40.Cm, 25.40.Ep, 24.10.Ht, 27.40.+z

I. INTRODUCTION

Several authors [1–4] have studied the (p,n) reaction at low energies on targets with mass number A near 100, 70, and 60. Analysis of these data showed that the volume integral of the absorptive potential at low bombarding energies was strongly dependent on A, with a sharp increase for nuclei between closed shells.

These results were confirmed by extensive work through studies of Ag, Mo, In, and Zr nuclei. The results confirmed that the volume integral of the absorptive part of the optical model potential (OMP) was strongly dependent on A. Additional work [5,6] showed that explicit inclusion of isospin does not significantly alter the A dependence of W. Further analysis of (p,p) and (p,n) cross sections on Zr and Mo isotopes, using a deformed potential coupling the ground and first excited states (2^+) of the target, only results in a 10–20% reduction of the absorptive volume integral, leaving the main features of the A dependence unchanged. Kailas *et al.* [4], studying the $A=60$ mass region, found a significant degree of correlation between β_2 and W. They also compared the *total* level density to W and found a significant degree of correlation.

Grimes [7] examined the role played by collective effects and the modulations of the density of intermediate states and found that the modulations with A in the two-particle–one-hole (2p-1h) state density are pronounced at 3-MeV proton energy but are markedly reduced at 6 MeV and above.

Cereda *et al.* [8], examining the A dependence of the absorptive potential concluded that there is no evidence of an anomalous behavior of W above the Coulomb barrier. This result can be explained by the findings of Grimes, since shell effects apparently disappear rapidly above the Coulomb barrier. Measurements of neutron elastic scattering at low energies [9] in the region $39<Z<51$ showed that W was strongly shell dependent with pronounced minima at $N=50$ and $Z=50$. The conclusion was less than half of this effect is due to collective motion.

In order to test these hypotheses, detailed studies of proton elastic and inelastic scattering on ^{54}Fe and ^{56}Fe at low energies were undertaken. ^{54}Fe has a closed neutron shell ($N=28$), a somewhat small β_2 (0.18), and exhibits vibrational behavior, while ^{56}Fe has a larger β_2 (0.24) and is well described by the asymmetric rotational model. Large negative (p,n) Q values and low (p,α) cross sections made the elastic channel dominant at low energy.

In the present work, proton elastic and inelastic differential cross sections have been measured at 3.73, 4.95, 6.06, and 7.74 MeV for ^{54}Fe and at 4.08, 5.02, 5.84, 6.56, and 7.74 MeV for ^{56}Fe. The (p,γ) cross section was also measured at the same energies. Proton elastic data are analyzed in the framework of the spherical optical model (SOM). The compound elastic scattering is subtracted from the total proton elastic scattering to obtain the proton shape elastic angular distributions. The potential strengths are optimized to obtain the best-fit parameters in a fixed geometry. Parameters obtained are used to predict the 2^+ proton inelastic cross sections and the (p,γ) data to check for consistency and to estimate the magnitude of the coupled-channels effects in the determination of the absorption cross section.

Previously published proton elastic scattering data [10] at higher energies were included in the data set to increase the energy range. The lower and higher energy OMP parameters are fitted with suitable functional forms which are used to estimate the dispersive contributions to the potential. The mean nuclear field obtained is compared with the available experimental single-particle (SP) binding energies. This dispersive OMP is then used to calculate the bound and unbound proton SP states in ^{55}Co and ^{57}Co. Experimental values for neutron bound SP states are obtained from single-nucleon transfer reactions having ^{55}Fe and ^{57}Fe as final states and are compared with those calculated from a neutron global OMP

*Present address: 1 Rve BenBrouk Hocine, Heliopolis, Guecma 24000, Algeria.
†Present address: Dept. of Radiation Oncology, Washington University, St. Louis, MO 63110.
‡Present address: Cyclotron Laboratory, Michigan State University, East Lansing, MI 48824.

potential. The complete set of SP states is used to calculate the 2p-1h state density in ^{55}Co and ^{57}Co. The importance of shell effects in the determination of the 2p-1h state density, and hence in the absorption cross section, is investigated.

II. EXPERIMENTAL METHOD

A. Proton scattering data

Differential proton elastic-scattering cross sections were measured at the Ohio University Tandem Van de Graaff facility. Details of beam production and acceleration have been extensively described elsewhere [11]. The experimental setup used to collect the data is identical to that of Dicello *et al.* [12].

The proton energy was accurately determined by bending the beam through a 90° analyzing magnet which is monitored by a nuclear magnetic resonance probe. Protons were detected with two surface-barrier silicon detectors. One, fixed at 135°, acted as a reaction monitor; the other could be rotated from 0° to 160° and was fitted with a 1-mm angle defining aperture and a movable antiscattering baffle to minimize slit-edge scattering [13]. With a target-to-detector distance of 15.5 cm, a maximum angular uncertainty of 0.4° is achieved.

Samples consisted of isotopically enriched ^{54}Fe and ^{56}Fe foils. Two sets of target thicknesses were required to carry out the measurements—the thin one for the lower half of the energy range ($E_p < 6$ MeV) and the thicker one for the higher energies ($6 < E_p < 8$ MeV). This was necessary in order to accommodate compound nucleus fluctuations which vary with excitation energy. At low energies, isobaric analog resonances (IAR) are well separated with large magnitudes, but they are fragmented and of smaller magnitude at the higher energies with a smaller energy separation between two consecutive fragments. It is necessary to avoid the large IAR at low energies but average out the less prominent fragments at the higher energies. ^{56}Fe samples were 99.9% pure, with thicknesses of 650 and 1.03 mg/cm^2. ^{54}Fe samples were 97.1% enriched with a 2.53% ^{56}Fe contamination and a 0.32% trace of ^{58}Fe. They were 664 and 1.04 mg/cm^2 thick.

Dead time corrections were made via a low-frequency pulser and were always small as care was taken during data collection in maintaining the beam current at low values. The largest corrections were of the order of 0.3% of any integrated peak.

Relative differential cross sections were obtained for carbon and oxygen from the experimental data at each angle where the corresponding elastic peaks are separated from the elastic peaks of iron. The contamination levels were calculated from the knowledge of the relative and absolute cross sections obtained from the OMP parameters. The total contamination level was found to be (1.0 ± 0.3)%.

Repeated measurements of Rutherford scattering ($E_p < 2$ MeV) showed that the deviations of the experimental data from the theoretical predictions were always less than 2%. The use of a fixed monitor detector allows a relative angular distribution to be obtained independent of possible target nonuniformities and without need for values for the absolute target thickness or solid angle of the detector. By assuming that the cross section for proton scattering is strictly Rutherford below 2 MeV, a value for the product of these factors can be found, allowing the high energy data to be normalized. An overall uncertainty of 4% in the scattering cross section was obtained.

B. (p,γ) measurements

For the proton capture reactions, the residual nuclei ^{55}Co and ^{57}Co have half-lives of 17.5 h and 271.8 days, respectively. In the decay of ^{55}Co, the 1.409-MeV ground-state transition from ^{55}Fe occurs with a 42% branching ratio. This transition was chosen as the "signature" because the efficiency of the detector at this energy (1.409 MeV) reaches a plateau and is less subject to uncertainty.

The ground state of ^{57}Co branches to the 136-keV excited state of ^{57}Fe with a 99.8% probability. This state then decays to the 14-keV excited state of ^{57}Fe with a branching ratio of 89% by the emission of a 122-keV γ ray. This γ ray was chosen as the "signature" because the detection efficiency is precisely known at this energy.

The γ-ray spectrometer used in the experiment consisted of a high-resolution intrinsic germanium crystal of cylindrical shape. A National Bureau of Standards [14] point source of mixed radionuclides provided an accurate full-energy-peak efficiency calibration of the germanium spectrometer for γ-ray energies between 40 and 1600 keV. The detector-to-sample distance was 5 cm, a reasonable value that eliminates the need for pulse-summing corrections [15] that occur when two γ rays strike the detector within the shaping time of the amplifier.

Before each run, a blank target measurement was carried out in order to estimate the natural background radiation and to make sure that no unwanted peak interfered with the data. The residual activity in the samples was measured before beginning activations and was found to be completely negligible. The electronics setup and dead time monitor was basically the same as for the proton data. A complete history of the activation of each target was maintained such that incremental activations at each energy were clearly isolated. Separate targets were used when the residual activity compromised the statistical accuracy of the incremental activations. Irradiations were for 10 h in the case of ^{54}Fe and 20 h in the case of ^{56}Fe at the same proton energies as those of the proton scattering data. The measurements were carried out in the same scattering chamber used to collect the proton scattering data, with the current integrated in a suppressed Faraday cup. The collected charge was checked against the monitor yields, which are accurately known from the proton scattering measurements. Charge integration was found to be better than 1%, as the intensity of the beam current ($\sim$500 nA) was much larger than any leakage current to the ground (which was $\sim$1–2 nA).

The main sources of uncertainty are due to the

efficiency calibration and the yield determination. The uncertainty in the efficiency ϵ is estimated to be less than 5%. The uncertainty in the yield was due mainly to the background subtraction and is estimated to be no greater than 5%. Statistical uncertainties were completely negligible as the typical integrated γ-ray peak had a very large number of counts. The data reported in Tables III and IV have an overall uncertainty which is estimated to be less than 10%.

III. PHENOMENOLOGICAL SPHERICAL OPTICAL MODEL

A. Introduction

A standard optical model with Woods-Saxon form factors, real spin orbit, and Coulomb potential was employed in calculating the cross sections. The determination of the OMP parameters was carried out in an iterative fashion. First, the model parameters are fitted to the elastic-scattering data using a reasonable starting geometry [16]. Next, comparisons are made between the experimental and the calculated cross sections for the various reaction channels in order to test the parameters obtained. The parameters of the OMP are then readjusted, the energy dependence is determined, and a second iteration between the calculated and the experimental values of the various reaction cross sections is carried out.

B. Compound elastic corrections

The Hauser-Feshbach [17] formalism, with and without Porter-Thomas width fluctuation corrections [18], was used to evaluate the compound nucleus contributions to the scattering. The open channels taken into consideration include both discrete states of known J^π and continuum states characterized by their level density parameters. The channels included in the calculations were (p,p), (p,p'), (p,n), (p,n'), (p,α), and (p,γ).

A multistep program, HF [19], was used to calculate the compound nucleus cross sections. The main effect of the width-fluctuation correction is to reduce the flux in all nonelastic channels, with a significant enhancement of the (p,p) compound elastic cross section.

Discrete states up to an excitation energy of 6.5 MeV in the residual nucleus were included in order to minimize the uncertainties due to the level density parameters. The J^π values for these states are found in the Nuclear Data Sheets [20,21]. The OMP parameters for the outgoing neutrons were from Ref. [22]. Those used for alpha particles where those of McFadden and Satchler [23].

The uncorrected data are first fitted with an optical model search routine to obtain optical model parameters which are then used in a Hauser-Feshbach calculation of the proton elastic cross section, which is subtracted from the measured data (following the method of Hansen *et al.* [24]). The resulting angular distribution is searched for the best OMP strengths, which are used in the next stage. It was necessary to use a width fluctuation correction for the lower energy data as the number of open channels is substantially smaller, and the formation and decay of the compound system are not completely independent processes. The iteration is continued, using the corrected data of the previous stage, until χ^2 and the transmission coefficients remained nearly constant. The algorithm converges after 2–3 iterations, provided the initial guesses for the OMP parameters are close to the actual values that describe the shape elastic scattering. The global OMP set for protons obtained by Becchetti and Greenless [16] were used as starting values.

In the case of ^{56}Fe, the (p,n) channel opens up at $E_p = 5.3$ MeV, and the level density parameters of ^{56}Co become important in the energy range between 5.3 and 8 MeV, as this channel increasingly dominates. The (p,p) compound elastic cross section peaks at $E_p \approx 5.5$ MeV, decreasing gradually with energy as the (p,n) and the (p,p') channels become more important. Inelastic scattering to the 2^+ state increases gradually with energy to reach a peak near $E_p = 5.80$ MeV, then decreases as the (p,n) reaction channel becomes more important. The (p,γ) channel is numerically unimportant when compared to the other reaction channels; however, it is useful in checking the accuracy of the compound nucleus corrections at the very low energies ($E_p = 4.08$ and 5.02 MeV).

In the case of ^{54}Fe, the threshold for the (p,n) reaction is 9.1 MeV, and the compound elastic and inelastic scattering are important below 9 MeV. Considerable difficulty was experienced in fitting the data at $E_p = 4.95$ and 6.06 MeV because of the presence of isobaric analog resonance contamination from $T_>$ states, particularly at backward angles. In general, one would expect to see resolved compound nucleus resonances only at low energies where their widths are less than their mean spacings. However, the IAR occur at high excitation energies and can still be quite narrow (~ 100 keV). Such resonances are distinguished from a continuous background of states by their isospin quantum number. These resonances can be seen in the high-resolution excitation functions that were measured by Lindstrom *et al.* [25] and Arai, Takahashi, and Kato [26]. They are fragmented in this energy region and their mean energy spacing is smaller than the energy loss of the incoming proton. As a result, it is not possible to average them out or to avoid them, and their presence introduces some distortion in the proton angular distributions, particularly at large angles. It was necessary to restrict the angular range for analysis to less than 135° for points at $E_p = 4.95$ and 6.06 MeV. The OMP parameters for these data points are not as reliable as those at other energies. The (p,γ) reaction is unimportant at proton energies greater than 3.5 MeV.

C. Analysis and results

The OMP computer program FOP [27] was used to fit the data. It can be seen from Figs. 1–3 that the OMP fits of the angular distributions at very low energies have very simple diffraction patterns, with a broad minimum. Because of this, the real radius parameter is not accurately determined. However, the value of r_r can be well

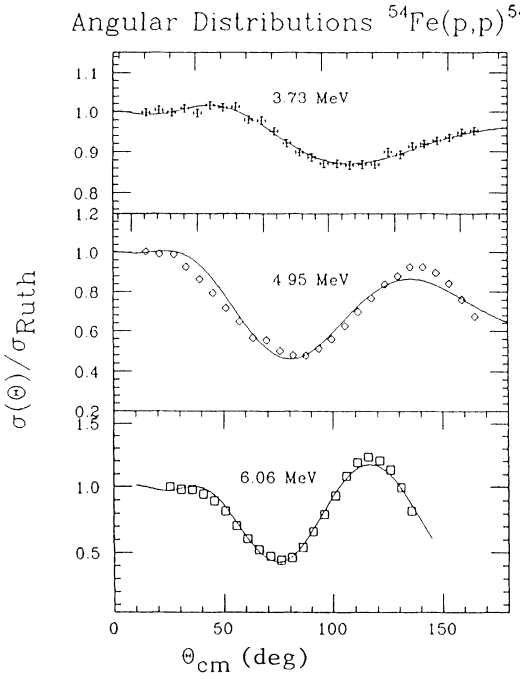

FIG. 1. Best OMP fit (solid line) for ^{54}Fe(p,p) at $E_p=3.73$, 4.95, and 6.06 MeV.

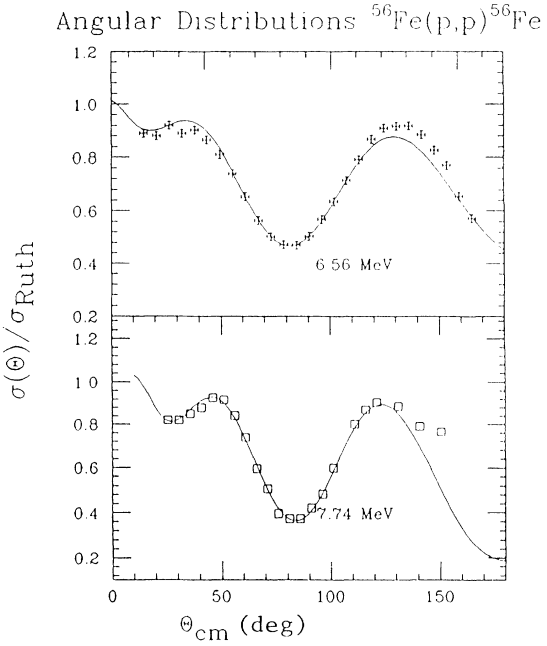

FIG. 3. Best OMP fit (solid line) for ^{56}Fe(p,p)^{56}Fe at $E_p=6.56$ and 7.74 MeV.

determined from analysis of the higher energy data and from the extrapolation of the potential to negative energies via the dispersion relation. The normalization constant is extracted from the Rutherford scattering that dominates at forward angles.

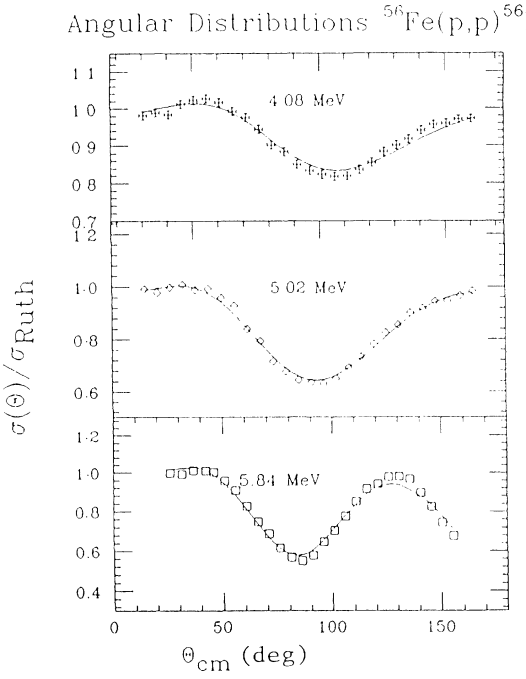

FIG. 2. Best OMP fit (solid line) for ^{56}Fe(p,p)^{56}Fe at $E_p=4.08$, 5.02, and 5.84 MeV.

After each search, the differential scattering cross sections are corrected for compound contributions, using the newly found values of the OMP. Individual best chi squared (χ^2) fits were first carried out, allowing the geometry of the central part of the potential (i.e., V_r, r_r, a_r, W_s, r_s, and a_s) to vary in order to determine the optimum parameters for the fixed geometry analysis that would accommodate both isotopes in order to make a useful comparison.

It was found that a value of $r_r=1.17$ fm fits the first minimum of the diffraction pattern quite well. The final choice for the geometry was

$$r_r=1.17 \text{ fm}, \quad r_s=1.32 \text{ fm},$$

$$a_r=0.70 \text{ fm}, \quad a_s=0.58 \text{ fm}.$$

These values are the same as those found in the global set for protons of Becchetti and Greenlees [16] except for the real diffuseness which is smaller in the present case. This similarity was expected as the parameters were required to provide a smooth transition from the lower to the higher proton energies. The diffuseness of the real volume term is smaller than that of Becchetti and Greenlees.

The values of the spin-orbit term of the OMP were not expected to play an important role at low energies [4]. Its inclusion in the search did not significantly alter the values of the potential strength. However, it is important to include it in order to fit the higher energy scattering data so that the dispersion relation calculations can be carried out and to determine the bound and unbound single-particle states that are needed in the 2p-1h calculations. Its values were kept fixed at the following, as

TABLE I. Best-fit proton optical model parameters for ^{56}Fe fixed geometry.

$r_r = r_v = 1.17$ fm $r_s = 1.32$ fm $r_{s.o.} = 1.04$ fm
$a_r = a_v = 0.70$ fm $a_s = 0.58$ fm $a_{s.o.} = 0.54$ fm
$V_{s.o.} = 5.75$ MeV

E_p (MeV)	V_r (MeV)	Error (%)	W_s (MeV)	Error (%)	W_v (MeV)	Error (MeV)	χ^2/N
4.08	56.67	1.8	6.85	11.4	0		0.31
5.02	56.88	0.68	7.01	3.7	0		0.17
5.84	60.10	0.31	8.08	2.8	0		0.92
6.56	57.38	0.35	9.24	2.9	0		2.0
7.74	54.11	0.47	9.01	2.6	0		0.79
17.2	52.10	0.41	6.42	5.1	0.90	51.5	9.0
20.4	51.3	0.38	7.82	4.7	0.95	49.0	7.0
35.2	44.7	1.50	5.33	13.7	4.23	34.4	38.0

determined from the analysis of the Eindhoven data [10]:

$$V_{s.o.} = 5.75 \text{ fm}, \quad r_{s.o.} = 1.04 \text{ fm}, \quad a_{s.o.} = 0.54 \text{ fm} .$$

The volume imaginary potential, W_v, is assumed to be zero for proton energies below 16 MeV. This is necessary as the search routine is not very sensitive to this parameter. The geometric parameters for this term are the same as those of V_r,

$$r_v = 1.17 \text{ fm}, \quad a_v = 0.70 \text{ fm} .$$

Fixing the geometry eliminates further uncertainties in the values of the potential strength that are introduced by the compound corrections as a_s and W_s values are crucial to the calculation of the compound elastic cross section. The fixed geometry best-fit parameters were obtained and checked for consistency against the (p,γ) and 2^+ scattering data. The various reaction channel cross sections are calculated with the Hauser-Feshbach code HF and are in good agreement with the experimental data. The parameters obtained are well fitted with linear analytic functions for proton energies below 10 MeV as follows: *Real central potential* (in units of MeV)

$$V_r(E) = V_0 - V_{er}E \quad (\text{for } E_p < 10 \text{ MeV}) ,$$

$$V_r(E) = \begin{cases} 61.75 - 0.44E & \text{for } ^{54}\text{Fe} , \\ 59.34 - 0.37E & \text{for } ^{56}\text{Fe} . \end{cases}$$

TABLE II. Best-fit optical model parameters for ^{54}Fe (same fixed geometry as for ^{56}Fe).

E_p (MeV)	V_r (MeV)	Error (%)	W_s (MeV)	Error (%)	W_v (MeV)	Error (%)	χ^2/N
3.73	58.77	1.28	4.60	11.7			0.83
4.95	61.60	0.36	5.51	7.0			6.85
6.06	62.80	0.29	6.34	6.5			2.1
7.74	55.77	0.53	9.42	3.74			3.07
17.2	52.70	0.66	6.12	4.56	1.93	18.6	9.70
20.4	51.05	0.36	6.41	3.47	5.3	19.8	2.1
35.2	45.87	0.83	3.28	7.8	6.71	8.45	4.13
40.0	45.69	0.58	4.97	6.02	4.06	13.1	7.0

Imaginary surface potentials (in units of MeV)

$$W_s(E) = W_{s.o.} + W_{es}E \quad (\text{for } E_p < 10 \text{ MeV})$$

$$W_s(E) = \begin{cases} -0.23 + 1.19E & \text{for } ^{54}\text{Fe} , \\ 3.85 + 0.72E & \text{for } ^{56}\text{Fe} . \end{cases}$$

The surface imaginary term slowly decreases with energy above 10 MeV, with its volume integral reaching an average value of 100 MeV fm^3. *Volume imaginary potential;* it is identically 0 for energies below 16 MeV. At a higher energy, the fit was improved by the inclusion of a volume component, but this remains the least well-determined part of the potential.

The potential strengths are listed in Tables I and II. The percentage errors are those assigned by the search routine and correspond to the percentage by which a parameter can be varied without changing χ^2 by one. The numerical values of the various reaction channels are presented in Tables III and IV.

D. Comparison with previous results

As indicated in the Introduction, a number of previous studies of the optical model parameters for low energy protons have been made. A recent summary of these results has been prepared by Mehta and Kailas [28]. As is pointed out by these authors, most such studies have been done on targets with small (p,n) Q values so that $\sigma(p,n)$ is approximately the absorption cross section at proton energies above 4 MeV. This criterion excludes the present targets so direct comparison is not possible. Neighboring nuclei have been studied by Kailas *et al.* [29] and Viyogi [30]. Because the geometrical parameters are slightly different, we compare the volume potential integral per nucleon. Both Kailas and Viyogi have volume integrals for the real potential which are $\frac{1}{2}$–1 % deeper for ^{56}Fe than ^{54}Fe (due to the $N-Z$ term). Our results have the real potential integral per nucleon 4% larger for ^{54}Fe. The present parameters also show a smaller change with energy, decreasing by 3% between 4 and 8 MeV, while the results of Kailas *et al.* and Viyogi drop by 8% over this interval. These small differences notwithstanding, the general agreement is quite good with agreement to within 5% at all energies between the three potential sets.

Such a comparison is not possible for the imaginary potential. As has been stressed by Mehta and Kailas [28] and Laird *et al.* [31], values of the imaginary potential at these energies have been found to vary as much as a factor of 5 for changes of 5–10 in A, but there is rapid convergence to smooth behavior as 10 MeV is approached. Our volume integrals per nucleon for the imaginary potential are 30% lower for ^{54}Fe than for ^{56}Fe at 4 MeV but are within 3% at 8 MeV, consistent with this trend. As previously mentioned, Refs. [29,30] do not include ^{54}Fe or ^{56}Fe data.

Finally, we note that other global potential sets, such as those of Becchetti and Greenlees [32], are often based entirely on data of 9 MeV and above. The Becchetti-Greenlees potential gives real potential integrals per nucleon which are in good agreement with the present results at 8 MeV (2% discrepancies) and are still fairly close

TABLE III. Summary table of the Hauser-Feshbach calculation for ^{56}Fe.

E_p (MeV)	σ_{elas} (mb)	σ_{2^+} (mb)	σ_{2^+} (expt) (mb)	$\sigma(p,\gamma)$ (mb)	$\sigma(p,\gamma)$ (expt) (mb)	$\sigma(p,n)$ (mb)	σ_{reac} (mb)
4.08	142.8	40.1	39.4	0.8	1.4		185
5.02	238.3	113.5	92.8	1.62	2.2		374
5.84	239.0	141.7	141.9	1.61	2.6	69.1	519
6.56	184.8	111.9	108.2	1.64	2.7	177.1	615
7.74	75.1	82.7	73.1	1.25		326	716

(5–6%) at the lowest energies. More problematic are the results for the imaginary potential, where the Becchetti-Greenlees results have the wrong slope with energy and are off by more than a factor of 2 for ^{54}Fe at 4 MeV and about a factor of 1.5 for ^{56}Fe at this energy. At 8 MeV, agreement is better than 10%. Clearly, the shell effects on the imaginary potential at these low energies are difficult to include in global optical potential sets.

IV. COUPLED-CHANNELS CALCULATIONS

In an early analysis, Perry [33] found a strong dependence of W_s on the coupling strength β. He also found that this effect is stronger at low energy. Tamura [34] showed that the inclusion of a nonspherical potential in the Schrödinger equation leads to a set of coupled differential equations for the radial wave function. It has been shown [35] that ^{54}Fe is well described by the vibrational model. The first 2^+ excited state is considered a one-phonon excitation; the next three excited states (4_1^+, 0_2^+, 2_2^+) are treated as two-phonon excitations, where these states are degenerate for an harmonic vibrator. ^{54}Fe is best described by the anharmonic vibrator, by introducing a one-phonon-like component into the 2_2^+ excitation [36].

The coupling strength of the 2_1^+ state was kept fixed at $\beta_2=0.18$. The higher-order parameters $\beta_3^1=0.132$ and $\beta_3^2=0.145$, corresponding to a coupling to 3^- states at 4.78 and 6.4-MeV excitation energy, were not expected to play an important role but were included in the calculation.

The low-lying states of ^{56}Fe are well described by the rotational model [37,38]. The Davydoff-Filipov asymmetric rotational model [39] was used, to describe the elastic scattering. A $(0^-,2_1^+,4_1^+,2_2^+)$ coupling scheme was used. Values of the band mixing coefficients $A_{ki}^i(\gamma)$ and the asymmetry parameters were those determined from the energy of the 2_1^+ and the 2_2^+ states as is done in Ref. [40].

The deformation parameter is $\beta_2=0.245$, as obtained by Delaroche *et al.* [41]. β_4 was taken as zero; it is not expected to play a significant role in the scattering [42]. Best-fit parameters resulting from coupled channel calculations of the elastic and 2^+ cross sections are shown in Tables V and VI.

In an extensive analysis of neutron and proton scattering on ^{54}Fe and ^{56}Fe, Mellema [42] has shown that at medium energy ($10 \le E_{nucleon} \le 30$ MeV) the elastic scattering was well described by a spherical optical model. The inclusion of deformed potentials made almost no difference in the elastic-scattering cross sections at these energies. At the present energies, comparison of the best-fit values for the imaginary potential shows large differences between the spherical and the coupled channel results, even though the calculated direct cross section for the 2^+ is small.

A. Analysis

The OMP parameters obtained from the spherical OMP were used in a coupled-channels calculation for each isotope to determine the importance of collective motion in the absorption cross section. The computer code ECIS79 [43] was used to search the corrected data with the ground state explicitly coupled to the first few excited states.

The low energy data set does not provide enough structure to allow a search on the deformation parameters to be carried out. If β is allowed to vary, the real well depth must be varied accordingly in order to match the first minimum with large uncertainties being introduced. For these reasons, it was thought wise to keep the parameters of the coupled channels fixed at the values obtained from the extensive study of ^{54}Fe and ^{56}Fe [42] at higher energy and allow only the potential strengths V_r and W_s to vary, with all the other OMP parameters fixed at the values ob-

TABLE IV. Summary table of the Hauser-Feshbach calculation for ^{54}Fe.

E_p (MeV)	σ_{elas} (mb)	σ_{2^+} (mb)	σ_{2^+} (expt) (mb)	$\sigma(p,\gamma)$ (μb)	$\sigma(p,\gamma)$ (expt) (μb)	σ_{reac} (mb)
3.73	93.9	7.4	8.8	68	79	101
4.95	231.4	60.5	58.6	76	87	301
6.06	283.3	131.3	175.1	105	119	506
7.74	203.2	147.1	134.6	220	202	722

TABLE V. Parameters of the functional form used in the dispersion relation calculations.

A	$V_{HF}(E_F)$ (MeV)	α_{HF}	C_1 (MeV)	d (MeV)	g (MeV)	C_2 (MeV)	h (MeV)
54	61.46	0.429	13.15	8.39	0.028	6.36	29.12
56	61.35	0.445	18.27	9.08	0.034	14.27	41.12

TABLE VI. Proton single-particle energies as calculated from the various terms of the dispersive optical model potential. The values indicated are the binding energies in MeV. Expt. stands for the experimental value.

State	V_{HF}	^{54}Fe $V_{HF}+\delta V_v$	$V_v+\delta V_s$	Expt.
$1f_{7/2}$	−4.70	−4.69	−4.66	−4.64
$2p_{3/2}$	−2.67	−2.41	−1.84	−1.37
$1f_{5/2}$	−1.76	−1.68	−0.95	−0.71
$2p_{1/2}$	−1.4	−1.3	−0.54	−0.28
State	V_{HF}	^{56}Fe $V_{HF}+\delta V_v$	$V_v+\delta V_s$	Expt.
$1d_{3/2}$	−13.8	−11.6	−10.9	−10.5
$1f_{7/2}$	−7.12	−6.69	−6.21	−6.02
$2p_{3/2}$	−5.11	−4.81	−4.14	−3.92
$1f_{5/2}$	−3.55	−3.05	−2.75	−2.19

tained from the phenomenological analysis. The higher energy data that were included [10] were also a part of the data set used in Mellema in his analysis.

B. Results and discussion

It was found that the fit to V_r is not significantly affected by the coupling, as the diffraction pattern has less structure than that of medium energy. At such low proton energies, the diffraction pattern, has, in general, only one minimum. However, a small adjustment of V_r was necessary to match the first minimum. As for W_s, the values obtained in the coupled-channels calculations are smaller than those of the spherical optical model calculations. These adjustments are justified when going from a purely spherical model to a deformed one, as flux is taken away because of the explicit inclusion of the excited states in the calculations. The magnitude of the decrease in W is of the order of 20%. This removal of flux actually enhances the absorption because the Coulomb barrier inhibits the decay of the 2^+ state. At low energies, the 2^+ state, once populated, has a very narrow decay width because of the Coulomb barrier and usually damps into the compound nucleus. At energies above the Coulomb barrier [7], inclusion of the 2^+ coupling tends to reduce the absorption cross section, i.e., its decay provides more competition and reduces the effect of the imaginary potential in producing compound nucleus formation. Thus, a smaller value for W in a coupled-channel calculation achieves the needed absorption, even though the direct excitation of the 2^+ state is very small.

V. DISPERSIVE OMP ANALYSIS

The dispersion relation (DR) has proved to be of great importance in several areas of physics. In the present work, the DR is used to check the energy dependence of the phenomenological OMP at the very low energies. This is necessary because the uncertainties introduced by large compound elastic subtractions to the elastic scattering do not allow optical model analysis to constrain the potentials. A full scope DR analysis would require a large body of experimental data. In particular, a more accurate knowledge of the single-particle energies is needed than is available. However, the main requirement is that the potential, with the dispersive contributions included, reproduce the experimental particle-hole gap, as obtained from single-nucleon transfer reactions, and this constraint will be used to obtain the energy dependence of the OMP potentials.

A. The dispersion relation constraint applied to the OMP

The DR equation can be expressed as [35,44]

$$V(r,E)=\mathcal{V}_{HF}(r,E)+\frac{\mathcal{P}}{\pi}\int_{-\infty}^{+\infty}\frac{\mathcal{W}(r,E')}{E'-E}dE'$$
$$=\mathcal{V}_{HF}(r,E)+\delta\mathcal{V}(r,E)\ ,$$

where $\mathcal{V}_{HF}(r,E)$ is the local equivalent of the nonlocal energy-dependent Hartree-Fock component of the nuclear mean field. $\mathcal{W}(r,E')$ is the absorptive part of the potential. The mean field is real at the Fermi energy E_F [45], hence,

$$\mathcal{W}(r,E_f)=0\ .$$

$\mathcal{W}(r,E)$ is assumed to be symmetric [46] with respect to the Fermi energy E_F:

$$\mathcal{W}(r,E'+E_F)=\mathcal{W}(r,-E'+E_F)\ .$$

This is a critical assumption which is reasonable for values of E that are close to the Fermi energy but is not realistic for values of E that are far from E_F. Haase and Schuck [47] have used an asymmetric absorptive potential which yields dispersive terms that are not symmetric with respect to E_F.

With the symmetric assumption, we get

$$\delta\mathcal{V}(r,E)=\frac{2}{\pi}(E-E_F)\mathcal{P}\int_{E_F}^{+\infty}\frac{\mathcal{W}(r,E')}{(E'-E_F)^2-(E-E_F)^2}dE'$$

and

$$\delta\mathcal{V}(r,E_F+E)=-\delta\mathcal{V}(r,E_F-E)\ .$$

We need to evaluate the dispersion integral for energies above the Fermi energy only.

The dispersive contribution to the potential can be separated out as

$$\delta\mathcal{V}(r,E)=\delta\mathcal{V}_v(r,E)+\delta\mathcal{V}s(r,E)\ .$$

These two contributions have an energy-dependent potential strength [$\delta V_v(E)$ or $\delta V_s(E)$] multiplying the corresponding r-dependent volume or surface form factor.

The central part of the dispersive OMP can be expressed as

$$\mathcal{V}(r,E)=\mathcal{V}_{HF}(r,E)+\delta\mathcal{V}_v(r,E)+\delta\mathcal{V}_s(r,E)\ .$$

In order to evaluate the dispersion integral, functional forms for $\mathcal{W}_v$ and $\mathcal{W}_s$ are needed. The best-suited energy-dependent representations were found to be

$$W_v(E)=C_2\frac{(E-E_F)^4}{(E-E_F)^4+h^4}(\text{MeV})$$

and

$$W_s(E)=C_1\frac{(E-E_F)^4}{(E-E_F)^4+d^4}e^{-g(E-E_F)}(\text{MeV})\ .$$

These forms have been shown by various workers [38,41,46] to be adequate for such calculations.

B. Analysis of the experimental data

The OMP geometrical parameters used in the analysis of the experimental scattering data were those determined in the phenomenological spherical OMP analysis. The phenomenological spherical OMP parameters were fitted with the functional forms listed above. The values of the parametrizations are listed in Table VII. The computer code BOUND [48] was used to carry out the calculations of the dispersive terms and the solutions of the one-body Schrödinger equation.

As for the extrapolation of the potential towards negative energies, the geometry was depth fixed for the reasons presented in Sec. III, with the additional constraint that the choice of r_r and a_r be suitable for the description of the single-particle bound states. In other words, the bound-state energies determined from the solution of the independent-particle model Schrödinger equation have to be in reasonable agreement with those determined from the single-nucleon transfer reactions. The calculated bound-state energies are quite sensitive to the real radius and diffuseness parameters. The particle-hole gap depends to a large extent on the strength of the spin-orbit term.

Scant experimental data on SP states in ^{54}Fe and ^{56}Fe are available. Furthermore, because of missing single-nucleon transfer data to some configurations at high excitation energy, a large amount of the strength is missed. For these reasons, it was decided to limit the number of the experimental SP energies to the very few states near the Fermi energy which is defined [44] as the average energy of the last occupied orbital with the first unoccupied orbital.

TABLE VII. Optical potential parameters obtained from coupled-channels analysis of proton elastic scattering on ^{56}Fe. The geometry is the same as that in the spherical OMP.

Fixed geometry

$r_r=r_v=1.17$ fm, $a_r=a_v=0.70$ fm, $r_s=1.32$ fm, $a_s=0.58$ fm, $r_{s.o.}=1.04$ fm, $a_{s.o.}=0.54$ fm, $V_{s.o.}=5.75$ MeV

E_p (MeV)	V_r (MeV)	W_s (MeV)	χ^2/N	$\sigma_{dir}(2^+)$ (mb)	σ_{react} (mb)
4.08	58.20	5.40	10.1	0.72	201.93
5.02	56.20	4.21	4.9	7.01	360.43
5.84	59.65	6.11	6.46	10.29	532.81
6.56	56.76	7.16	9.33	12.71	628.73
7.74	52.12	7.94	36.67	16.12	751.43

TABLE VIII. Optical potential parameters obtained from coupled-channels analysis of proton elastic scattering on ^{54}Fe. The geometry is the same as that in the spherical OMP.

E_p (MeV)	V_r (MeV)	W_s (MeV)	χ^2/N	$\sigma_{dir}(2^+)$ (mb)	σ_{react} (mb)
3.73	57.05	3.48	1.60	0.01	121.6
4.95	62.62	4.93	5.97	0.80	328.6
6.06	61.64	5.38	7.90	4.49	516.1
7.74	55.50	6.75	5.31	8.94	699.3

The experimental SP binding energies, as obtained from single-nucleon transfer reactions, are from Refs. [49,50]. Their numerical values, as well as the results of the DR calculations, are presented in Table VIII.

The following method was used to compare the experimental SP states to those obtained from an extrapolation of the dispersive mean field [46]. The extrapolated values of $V(E_{nlj})=V_{HF}(E_{nlj})+\delta V_v(E_{nlj})$ were used to calculate the SP binding energy. The surface dispersive term $\delta V_s(E_{nlj})$ is calculated separately. Agreement with the experimental SP energies is significantly improved when this term is included in the Schrödinger equation. In particular, the particle-hole gap values that are obtained from the DR are in good agreement with the experimental values. The calculated values are 3.3 MeV for ^{55}Co and 2.1 MeV for ^{57}Co. The experimental values, as obtained from single-nucleon transfer reactions, are 3.27 MeV for ^{55}Co and 2.1 MeV for ^{57}Co. The proton separation energy is 5.05 MeV for ^{55}Co and 6.03 MeV for ^{57}Co.

C. Discussion and conclusions

The particle-hole gap, δ_{ph}, and the experimental SP binding energies in the immediate vicinity of the Fermi energy are well reproduced by the dispersive OMP. These calculations were not intended to be a full-scope study of the role of dispersion relation effects in the scattering but were only used to check the goodness of the phenomenological OMP parameters obtained in Sec. III, as well as their energy dependence. This was thought to be necessary as the OMP parameters obtained in the preceding sections may have large uncertainties due to the compound elastic corrections and possibly isobaric analog contaminations in the differential elastic-scattering cross sections. The results of this section enhance the confidence in the 2p-1h state density calculations which is quite sensitive to the particle-hole gap value.

VI. PARTICLE-HOLE CALCULATIONS

The present calculations are based on the exciton model of Griffin [51], as extended by Blann [52] and Williams [53]. The basic assumption of this model is that formation of the compound nucleus proceeds via stages attained solely through sequential two-body interactions. At each stage a finite probability exists for the particle-hole configuration to decay through the emission of a particle or damp into more complicated configurations.

This model assumes that the level densities for various particle-hole states can be calculated from the SP states. The SP states are classified according to the number of particles and holes (called "excitons") which are excited from the ground state. The details of the two-body interaction are suppressed by replacing all the nonvanishing matrix elements by an average value.

A. Calculation of the 2p-1h state density

The basis of proton SP states was generated from the mean nuclear potential obtained in Sec. III. The computer code BOUND [48] was used to calculate the bound SP energies. The unbound SP states were calculated with the same dispersive OMP with an artificially small W_s ($W_s = 0.5$ MeV) in order to make the SP resonances observable in the transmission coefficients. It is to be noted that the location of these unbound SP states are shifted to a higher energy by approximately 1 MeV when the real part of the OMP is allowed to depend on the energy. It is assumed that the uncertainty in these SP energies is of the same magnitude. The uncertainty in the bound-state energies is estimated to be 1 MeV.

Experimental spectroscopic factors obtained from single-nucleon transfer reactions show an energy gap of 3.27 MeV between the $f_{7/2}$ and the $2p_{3/2}$ proton shells in ^{55}Co. This gap is smaller for ^{57}Co and is equal to 2.10 MeV.

As for the neutron single-particle states, no information exists for such odd systems as ^{55}Co and ^{57}Co. Single-nucleon transfer reaction data provide information on some bound states in ^{55}Fe and ^{57}Fe and the isobaric analog to the ground state in ^{55}Co and ^{57}Co. According to Rapaport's global neutron potential [22], the well depth of the potential corresponding to the isobaric pairs should not differ by more than a few hundred keV as the values of $(N-Z)/A$ are practically the same. This approach was taken by Lawson, Guenther, and Smith [54]. The unbound neutron SP states were calculated using the global neutron potential mentioned above.

A computer program, PHDENS [55], was developed in order to carry out the calculations of the particle-hole state densities. This program calculates particle-hole configurations up to 4p-4h using combinatorial methods based on the exciton model.

B. Discussion and results

The assumption that the nuclear force is two body in nature leads to the conclusion that the first step in the formation of a compound nucleus is a damping of the single-particle state into a two-particle–one-hole state. Just as is found for total level densities, such an exciton level density (exciton number denotes the sum of the particle and hole number) would be expected to show shell effects. Particularly at low energies, nuclei close to or at closed shells should have reduced densities of such states compared to nuclei more removed from closed shells. A recent study of the exciton level densities of ^{56}Fe by Reffo and Herman [56] showed that the energy shifts varied somewhat with exciton number.

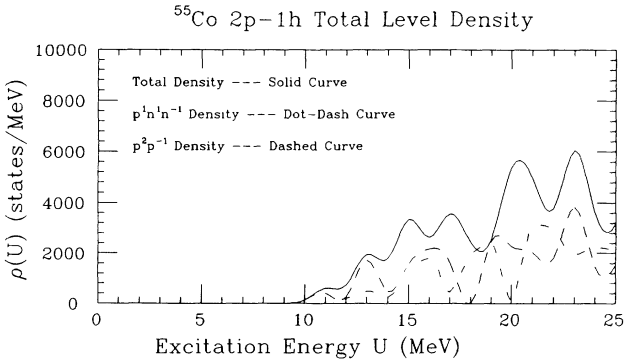

FIG. 4. ^{55}Co 2p-1h total level density including all possible values of angular momentum and parity.

The resulting two-particle–one-hole state densities for ^{55}Co and ^{57}Co were averaged with a Gaussian convolution function of width 1.5 MeV. This should simulate the effects of the two-body interaction. By unitarity, the total number of states will be conserved, so the effect of the two-body interaction will be to shift the strength in energy and remove the large degeneracies characterizing the noninteracting system.

Calculated values for the two-particle–one-hole densities are shown in Figs. 4–8. The calculation includes all spins and both parities, but because the penetrability of waves of $l=3$ and higher is small, a more meaningful comparison is for level densities of $J \leq \frac{5}{2}$. Note that this restriction reduces the densities by more than a factor of 3, but it leaves unchanged the result that the low energy density for ^{55}Co is very much less than for ^{57}Co, while as the energy increases the two converge to some degree. The restriction to $J \leq \frac{5}{2}$ is supported by the tabulations in Tables IX and X. Note that the $f_{7/2}$ component is always less than 10% of the cross section and untabulated partial waves of $l \geq 4$ are less than 8%.

For a uniform single-particle state distribution, the two-particle–one-hole state distribution would have the energy dependence CU^2, where U is the energy. In a study of preequilibrium reactions, Grimes *et al.* [57,58]

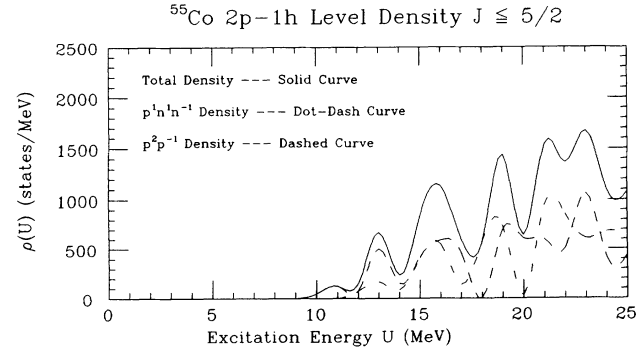

FIG. 5. ^{55}Co 2p-1h level density with angular momentum restrictions.

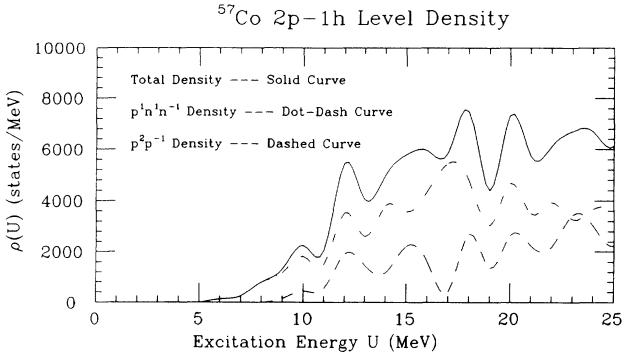

FIG. 6. ^{57}Co 2p-1h level density including all possible values of angular momentum and parity.

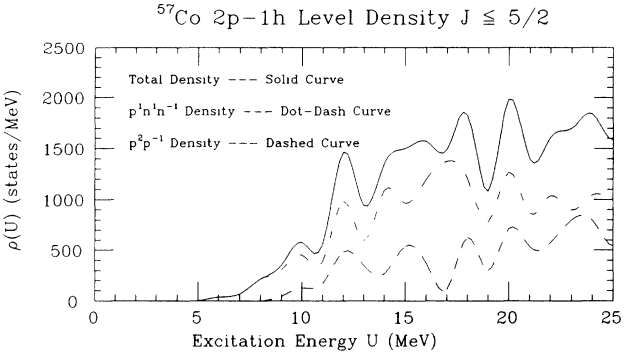

FIG. 7. ^{57}Co 2p-1h level density with angular momentum restrictions.

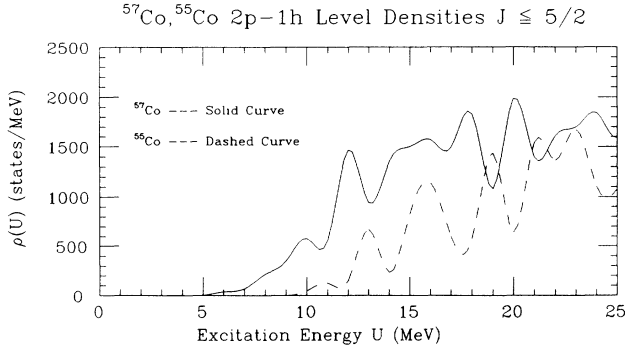

FIG. 8. 2p-1h level densities in ^{55}Co and ^{57}Co with angular momentum restrictions.

TABLE IX. Partial reaction cross sections calculated from OMP transmission coefficients. The numbers in rows correspond to the percentage of the contribution to the total reaction cross section for each individual wave at each scattering energy E_p.

	^{56}Fe						
E_p (MeV)	$S_{1/2}$ (%)	$P_{1/2}$ (%)	$P_{3/2}$ (%)	$D_{3/2}$ (%)	$D_{5/2}$ (%)	$F_{5/2}$ (%)	$F_{7/2}$ (%)
4.08	35.8	11.9	17.7	10.0	20.2	2.1	1.6
5.02	28.5	7.0	12.9	15.6	29.9	2.0	2.6
5.84	19.7	6.6	13.6	19.5	30.4	2.9	4.7
6.56	15.6	6.9	13.6	18.9	19.4	4.5	6.8
7.74	11.6	6.4	11.8	17.7	28.0	7.3	9.5

have found use of realistic single-particle state energies results in a better fit with the form $C(U-\delta)^2$, where δ is a shell and pairing energy shift. Inspection of the figures shows that this shift will be larger for ^{55}Co (δ_1) than for ^{57}Co (δ_2). As the energy increases, the relative difference between the two level densities decreases, as $U \gg \delta_1$ or δ_2. To make a meaningful comparison, the density for ^{55}Co at E_p+5 MeV needs to be compared with that for ^{57}Co at E_p+6 MeV, since these are the separation energies. Calculating the ratio between the two densities with the appropriate energy shift yields a function with substantial oscillations, but an averaged calculation yields ratios ranging from about 2.5 at energies corresponding to 5-MeV protons to 1.25 at 9 MeV for level density of ^{57}Co to that for ^{55}Co. A more quantitative treatment which treated the two-body force more exactly would be desirable, as would a comparison that included weighting to account for the different strength of the p-n and p-p interactions as well as weighting the different J's appropriately. Nonetheless, the calculation does predict a higher absorption for a ^{56}Fe target than for ^{54}Fe at low energy and a gradual approach to equality as the energy increases.

VII. SUMMARY AND CONCLUSIONS

The proton scattering data were analyzed in the framework of the phenomenological OMP with a fixed geometry. The elastic differential cross sections were fitted quite well except for some high energy data points

TABLE X. Partial reaction cross sections calculated from OMP transmission coefficients. The numbers in rows correspond to the percentage of the contribution to the total reaction cross section for each individual wave at each scattering energy E_p.

	^{54}Fe						
E_p (MeV)	$S_{1/2}$ (%)	$P_{1/2}$ (%)	$P_{3/2}$ (%)	$D_{3/2}$ (%)	$D_{5/2}$ (%)	$F_{5/2}$ (%)	$F_{7/2}$ (%)
3.73	59.3	3.3	5.9	6.7	23.1	0.4	0.6
4.95	31.7	5.4	10.3	15.2	32.9	1.3	1.9
6.06	18.7	5.5	11.8	22.1	32.8	2.5	4.3
7.74	11.8	6.4	12.2	18.0	27.9	6.7	9.2

in the backward direction. This is attributed to the fact that the geometry of the OMP is fixed and at higher energies the spin-orbit term of the potential becomes important particularly in the backward direction. The phenomenological OMP parameters were fitted with functional forms that are suitable for both the Hauser-Feshbach and the dispersion relation calculations. The OMP parameters were used to calculate the compound 2^+ inelastic cross sections and the (p,γ) cross sections. As seen in Tables III and IV, these calculated values were in reasonable agreement with the corresponding measured data. The volume integrals obtained from the phenomenological OMP agree with those obtained from the global set of Kailas *et al.* [4].

The SOM potential parameters were used in coupled-channels calculations in order to investigate the role played by collective motion in the mass dependence of W_s. Explicit coupling of the ground state to the 2^+ excited state results in a 10–20% increase in the reaction cross section at the very low energies and a decrease in the reaction cross section at higher energies. This is in agreement with the findings of Refs. [7,9]. However, there are some limitations to these calculations: ^{54}Fe and ^{56}Fe are not highly collective nuclei and the difference in their coupling strengths (β_2) is rather small.

The dispersive contributions to the OMP were estimated and used to extrapolate the potential to negative energies. Most importantly, the particle-hole gaps and the Fermi energies obtained from the dispersion relation calculations agreed with the experimental values within 5%. These are sensitive parameters in a 2p-1h state density calculations.

The mean nuclear field was used to calculate the SP state energies in ^{55}Co and ^{57}Co, the compound nuclei formed by proton bombardment of ^{54}Fe and ^{56}Fe. The density of doorway states was calculated using these basis in the framework of the exciton model. The total 2p-1h state density for ^{55}Co turned out to be much smaller than that of ^{57}Co, particularly below 12-MeV excitation energy. Asymptotically, the 2p-1h state density reaches the same order of magnitude for both nuclei as a function of energy. For each measured angular distribution, the total reaction cross section was broken down into partial reaction cross sections corresponding to the various partial waves (T_{lj}). Angular momentum and parity restrictions were applied to the 2p-1h state density, allowing only those J^π values that have a significant contribution to the total reaction cross sections. It is seen in Tables V and VI and Fig. 8 that there is a high degree of correlation between the magnitude of W_s and the density of the 2p-1h states when comparing ^{55}Co and ^{57}Co.

The main conclusion is that the modulation of the 2p-1h state density induced by shell closure appears to be largely responsible for the observed mass dependence of the imaginary strength, W_s, of the OMP. The collective effects may contribute but are rather small (less than 20%) in magnitude.

[1] C. H. Johnson, J. K. Bair, C. M. Jones, S. K. Penny, and D. W. Smith, Phys. Rev. C **15**, 196 (1977).

[2] C. H. Johnson, A. Galonsky, and R. L. Kernel, Phys. Rev. Lett. **39**, 604 (1979); Phys. Rev. C **20**, 2052 (1979).

[3] D. S. Flynn, R. L. Hershberger, and F. Gabbard, Phys. Rev. C **20**, 1700 (1979).

[4] S. Kailas, M. K. Mehta, S. K. Gupta, Y. P. Viyogi, and N. K. Ganguly, Phys. Rev. C **20**, 1272 (1979).

[5] R. Schrils, D. S. Flynn, R. L. Hershberger, and F. Gabbard, Phys. Rev. C **20**, 1706 (1979).

[6] D. S. Flynn, R. L. Hershberger, and F. Gabbard, Phys. Rev. C **26**, 1744 (1982).

[7] S. M. Grimes, Phys. Rev. C **22**, 436 (1980).

[8] E. Cereda, M. Pignanelli, S. Micheletti, H. V. von Geramb, M. N. Harakeh, R. DeLeo, G. D'Erasmo, and A. Pantaleo, Phys. Rev. C **26**, 1941 (1982).

[9] A. B. Smith, P. T. Guenther, and J. F. Whalen, Nucl. Phys. A **415**, 1 (1984).

[10] P. J. Van Hall, J. P. M. G. Melssen, S. D. Wassenaar, O. J. Poppema, S. S. Klein, and G. J. Nijgh, Nucl. Phys. A **291**, 63 (1977).

[11] D. E. Bainum, Ph.D. dissertation, Ohio University, 1977.

[12] J. F. Dicello, G. Igo, W. T. Leland, and F. G. Perey, Phys. Rev. C **4**, 1130 (1971).

[13] F. G. Resmini, A. D. Bacher, D. J. Clark, E. A. McClatchie, and R. DeSwiniarski, Nucl. Instrum. Methods **74**, 261 (1969).

[14] S. R. Rasberry, *Mixed-Radionuclide Point-Source Standard for the Efficiency Calibration of Germanium-Spectrometer Systems,* Nat. Bur. Stand. Ref. Data Ser., Natl. Bur. Stand. (U.S.) Cir. No. SRM 4725-B-43 (U.S. GPO, Washington, D.C., 1983).

[15] K. Debertin and U. Sholtzig, Nucl. Instrum. Methods **158**, 471 (1979).

[16] F. D. Becchetti and G. W. Greenlees, Phys. Rev. **182**, 1190 (1969).

[17] W. Hauser and H. Feshbach, Phys. Rev. **87**, 366 (1952).

[18] C. E. Porter and R. G. Thomas, Phys. Rev. **104**, 483 (1956).

[19] S. M. Grimes, J. D. Anderson, J. W. McClure, B. A. Pohl, and C. Wong, Phys. Rev. C **10**, 2373 (1974).

[20] R. L. Auble, Nucl. Data Sheets **20**, 253 (1977).

[21] L. K. Peker, Nucl. Data Sheets **42**, 457 (1984).

[22] J. Rapaport, V. Kulkarni, and R. W. Finlay, Nucl. Phys. A **330**, 15 (1979).

[23] L. McFadden and G. R. Satchler, Nucl. Phys. **84**, 177 (1966).

[24] L. F. Hansen, S. M. Grimes, J. L. Kammerdiener, and V. A. Madsen, Phys. Rev. C **8**, 2072 (1973).

[25] D. P. Lindstrom, H. W. Newson, E. B. Bilpuch, and G. E. Mitchell, Nucl. Phys. A **168**, 37 (1971).

[26] E. Arai, T. Takahashi, and J. Kato, Nucl. Phys. A **324**, 63 (1979).

[27] F. S. Dietrich, Lawrence Livermore National Laboratory, California (1983).

[28] M. K. Mehta and S. Kailas, Pramana **27**, 139 (1986).

[29] S. Kailas, S. K. Gupta, M. K. Mehta, S. S. Kerekatte, L. V. Namjoshi, N. K. Gauquly, and S. Chintalapudi, Phys. Rev. C **12**, 1789 (1975).

[30] Y. P. Viyogi, Ph.D. thesis, Calcutta University, 1983, as

quoted in Ref. [28].
[31] C. E. Laird, D. Flynn, R. Hershberger, and F. Gabbard, Phys. Rev. C **35**, 1265 (1987).
[32] F. D. Becchetti and G. W. Greenlees, Phys. Rev. **182**, 1190 (1969).
[33] F. G. Perey, Phys. Rev. C **131**, 745 (1963).
[34] T. Tamura, Rev. Mod. Phys. **37**, 679 (1965).
[35] J. P. Delaroche, Y. Wang, and J. Rapaport, Phys. Rev. C **39**, 391 (1988).
[36] T. Tamura, Suppl. Prog. Theor. Phys. **37**, 383 (1966).
[37] J. P. McGrory and S. Raman, Phys. Rev. C **20**, 830 (1979).
[38] D. G. Sarantites, J. Urbon, and L. L. Rutledge, Jr., Phys. Rev. C **14**, 1412 (1976).
[39] A. S. Davydoff and B. F. Filipov, Nucl. Phys. **8**, 237 (1958).
[40] J. M. Eisenberg and W. Greiner, *Nuclear Models* (North-Holland, Amsterdam, 1975), p. 168.
[41] J. P. Delaroche, S. M. El-Kadi, P. P. Guss, C. E. Floyd, and R. L. Walter, Nucl. Phys. A **390**, 541 (1982).
[42] S. H. Mellema, Ph.D. dissertation, Ohio University, 1983; S. H. Mellema, R. W. Finlay, and F. S. Petrovich, Phys. Rev. C **28**, 2267 (1983).
[43] J. Raynal, ECIS79, 1979 (unpublished).
[44] C. Mahaux and R. Sartor, *Advances In Nuclear Physics,* edited by J. W. Negele and E. Bogt (Plenum, New York, 1992), Vol. 20, p. 1.
[45] J. P. Jeukenne, A. Lejeune, and C. Mahaux, Phys. Lett. **59B**, 208 (1975).
[46] C. Mahaux and H. Ngo, Nucl. Phys. A **378**, 205 (1982).
[47] R. W. Hasse and P. Schuck, Nucl. Phys. A **438**, 157 (1985); **445**, 205 (1985).
[48] R. K. Das, Ph.D. dissertation, Ohio University, 1988.
[49] Z. Enchen, H. Junde, Z. Chunmei, L. Xiane, and W. Lizheng, Nucl. Data Sheets A **44**, 55 (1985).
[50] T. W. Burrows and M. R. Bhat, Nucl. Data Sheets A **47**, 57 (1986).
[51] J. J. Griffin, Phys. Rev. Lett. **17**, 478 (1966).
[52] M. Blann, Phys. Rev. Lett. **21**, 1357 (1968).
[53] F. C. Williams, Jr., Phys. Lett. **31B**, 184 (1970).
[54] R. D. Lawson, P. T. Guenther, and A. B. Smith, Phys. Rev. C **36**, 1298 (1987).
[55] S. M. Grimes and N. Boukharouba, computer program PHDENS, 1991 (unpublished).
[56] M. Herman and G. Reffo, Phys. Rev. C **36**, 1546 (1987).
[57] S. M. Grimes, J. D. Anderson, J. W. McClure, B. A. Pohl, and C. Wong, Phys. Rev. C **7**, 343 (1973).
[58] S. M. Grimes, J. D. Anderson, and C. Wong, Phys. Rev. C **13**, 2224 (1976).